JACS
JOURNAL OF THE AMERICAN CHEMICAL SOCIETY
Article
pubs.acs.org/JACS

Understanding Fluxes as Media for Directed Synthesis: *In Situ* Local Structure of Molten Potassium Polysulfides

Daniel P. Shoemaker,[†] Duck Young Chung,[†] J. F. Mitchell,[†] Travis H. Bray,[‡] L. Soderholm,[‡] Peter J. Chupas,[¶] and Mercouri G. Kanatzidis*[,§,†]

[†]Materials Science Division, [‡]Chemical Sciences and Engineering Division, and [¶]X-ray Science Division, Argonne National Laboratory, Argonne, Illinois 60439, United States

[§]Department of Chemistry, Northwestern University, Evanston, Illinois 60208, United States

ABSTRACT: Rational exploratory synthesis of new materials requires routes to discover novel phases and systematic methods to tailor their structures and properties. Synthetic reactions in molten fluxes have proven to be an excellent route to new inorganic materials because they promote diffusion and can serve as an additional reactant, but little is known about the mechanisms of compound formation, crystal precipitation, or behavior of fluxes themselves at conditions relevant to synthesis. In this study we examine the properties of a salt flux system that has proven extremely fertile for growth of new materials: the potassium polysulfides spanning K_2S_3 and K_2S_5, which melt between 302 and 206 °C. We present *in situ* Raman spectroscopy of melts between K_2S_3 and K_2S_5 and find strong coupling between n in K_2S_n and the molten local structure, implying that the S_n^{2-} chains in the crystalline state are mirrored in the melt. In any reactive flux system, K_2S_n included, a signature of changing species in the melt implies that their evolution during a reaction can be characterized and eventually controlled for selective formation of compounds. We use *in situ* X-ray total scattering to obtain the pair distribution function of molten K_2S_5 and model the length of S_n^{2-} chains in the melt using reverse Monte Carlo simulations. Combining *in situ* Raman and total scattering provides a path to understanding the behavior of reactive media and should be broadly applied for more informed, targeted synthesis of compounds in a wide variety of inorganic fluxes.

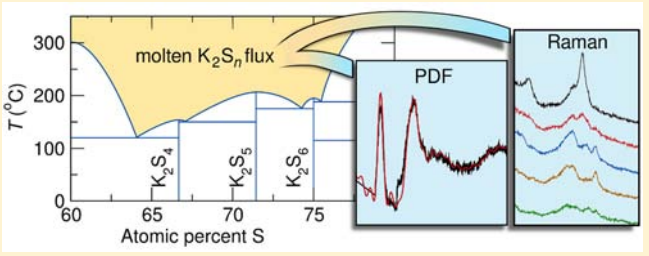

INTRODUCTION

The concept of inorganic materials synthesis by design is predicated on the ability to control the formation of metastable phases. This is a particular challenge in the creation of energy-relevant inorganic materials, where slow diffusion rates are often countered by high-temperature reactions which produce only the thermodynamically stable products. This is epitomized in the case of oxides, which are commonly refractory due to strong ionic bonding.

A more desirable approach would share the advantages of organic synthesis: low-temperature reactions and gentler chemistry allow the selective assembly of tailored molecules. In solid-state chemistry the closest approximation is reactive flux synthesis, where a low-melting element (In, Ga, Sn, S, etc.) or salt (oxide, other chalcogenide, halide) permits facile diffusion and may take part in the reaction itself. Especially when salts of the less electronegative chalcogenides (S, Se, or Te) are used, the combination of gentle cation−anion bonding and low melting temperatures permits the formation of many novel or metastable phases.[1−3] Despite the versatility of these reactions and the vast array of products discovered, little is known about the reaction mechanisms, species present in the flux, or the behavior of the flux itself at high temperatures.

The ability to selectively nucleate complex phases is aided when a flux not only maintains diffusion but is an integral part of the reaction itself. For that reason we focus on fluxes of the molten alkali polychalcogenides (A_2Q_n, where A is an alkali metal and Q a chalcogenide) which exhibit low melting temperatures and Q−Q bonding. Interactions between the solvent and the solute allow the formation of phases that are unattainable by direct combination of their constituents.[4−11] Reactions in these fluxes have produced promising new materials for use in photovoltaics,[12−14] thermoelectrics,[15−18] nonlinear optics,[13,19−21] and heavy metal and nuclear waste remediation.[22,23] Alkali species in the flux can dismantle a preformed structure, leading to tunable properties by a process known as dimensional reduction.[24,25] It is also possible for structural motifs from the flux itself to be incorporated in the final product.[26,27] But how do these compounds form, and from what?

Only one study by Dürichen and Bensch has attempted to probe reaction mechanisms in a polyanionic flux.[28] They found that Nb in K_2S_n fluxes at 350 °C gave four products for varying n, but only *ex situ* measurements were performed. There is no consensus on suitable methods to characterize these systems at conditions relevant to crystal growth. Attempts to model the stability of polyanionic species have been limited to the gas

Received: March 29, 2012
Published: May 14, 2012

   dx.doi.org/10.1021/ja303047e | *J. Am. Chem. Soc.* 2012, 134, 9456−9463

phase,[29,30] but these isolated molecules do not share the structure or stability of their counterparts in liquid salts.[31]

In order to understand, and eventually control, directed syntheses of inorganic materials in molten fluxes, it is first necessary to characterize the reaction medium. Once details are known about chemical species contained in the flux, behavior of these species can be monitored *in situ* to understand mechanisms of crystal growth and compound formation.

In this study we examined the K_2S_n flux system due to its demonstrated utility for low-temperature reactions with many metals.[12,28,33−35] The K−S phase diagram in Figure 1 reveals ionic salts K_2S_n, where $1 \leq n \leq 6$.[32] The shaded region indicates compositions where a low-melting flux can be used as a medium for crystal growth.

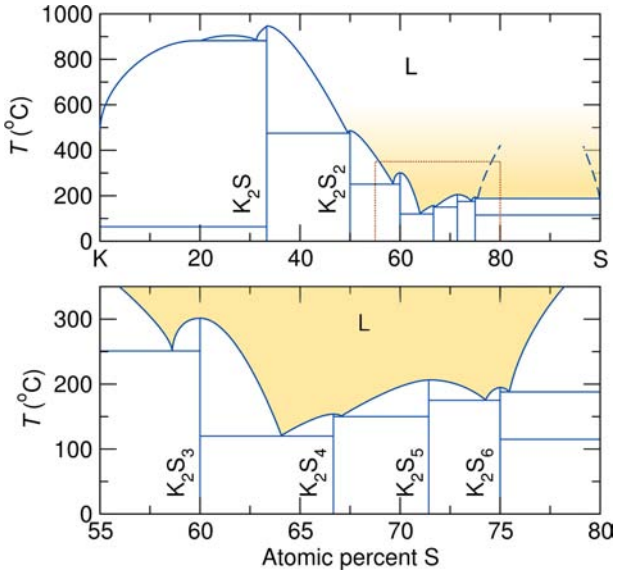

Figure 1. K−S phase diagram containing the low-melting compounds K_2S_3 (T_m = 302 °C), K_2S_4 (T_m = 154 °C), which is glassy, K_2S_5 (T_m = 206 °C), and K_2S_6 (T_m = 183 °C). Adapted from Sangster;[32] dotted region is shown as an inset in the bottom pane. The shaded region represents conditions where the low-melting flux may enable controlled growth of new materials.

The fluxes K_2S_3 and K_2S_5 crystallize to form chains of S_n^{2-} polyanions. Unit cells of these two compounds are shown in Figure 2. The distribution of these chains in the melt and their response to the addition of reagents should be important factors in the growth of new phases.

Large distributions of S_n^{2-} chain lengths were predicted in molten Na_2S_n to explain the electromotive force in Na−S batteries, which is nearly linear versus n, but these were not substantiated by any structural or spectroscopic techniques.[36,37] In fact, neither conductivity nor density of Na_2S_n varies smoothly over the same range.[38,39]

We utilized *in situ* high-temperature Raman spectroscopy to probe S_n^{2-} chain formation in molten K_2S_n. Previous Raman studies have only examined solid polysulfides[40,41] and solutions of S_n^{2-} in liquid ammonia.[40,42−44] Our Raman analysis does not support Na−S battery models which propose molten S_n^{2-} to exhibit a wide range of chain lengths in equilibrium. Instead we find that the melt structure is highly dependent on stoichiometry.

We investigated the real-space structure of K_2S_5 melts using *in situ* high-temperature X-ray total scattering to obtain the pair

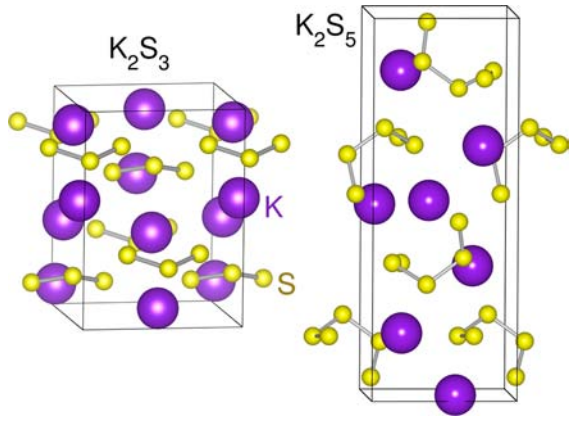

Figure 2. Unit cells of K_2S_3 ($Cmc2_1$, 7.31 × 9.91 × 7.47 Å) and K_2S_5 ($P2_12_12_1$, 6.49 × 6.60 × 17.41 Å) containing polysulfide chains of S_3^{2-} and S_5^{2-} respectively, shown here connected by bonds.

distribution function (PDF). The PDF provides atom−atom distances in real space, regardless of the disappearance of long-range symmetry in the melt.[45] We employed large-box reverse Monte Carlo (RMC) simulation of the PDF, which is crucial for investigating highly disordered materials.[46−48] A chain-building algorithm was developed to probe the formation of S_n^{2-} polyanions. At present this technique cannot independently resolve S_n^{2-} chain lengths in molten K_2S_5, but it should have utility for fluxes with smaller or more rigid polyanions.

EXPERIMENTAL PROCEDURE

Potassium polysulfides were prepared using a crucible-in-tube technique. This technique avoids direct contact between K and S, which can react violently, and is a safe, one-step alternative to synthesis in liquid ammonia.[32] Elemental K (Aldrich, 99.5%) was placed in the bottom of an 18-mm-diameter quartz tube. Elemental S (Cerac, 99.999%) was placed in a 2-mL cylindrical Al_2O_3 crucible resting on indentations approximately 2 cm above the K. The tube was flame-sealed under vacuum while the K-containing end was submerged in liquid nitrogen to prevent reaction during the sealing process. Tubes were heated upright in a box furnace with a 12-h ramp to 300 °C, at which point the S had vaporized and reacted with K to form a melt (brown for K_2S_3, dark red for K_2S_5). The tube was removed from the furnace while hot, then cracked open in a N_2-filled glovebox for collection of the product.

High-resolution synchrotron X-ray powder diffraction patterns were collected using the mail-in configuration of beamline 11-BM at the Advanced Photon Source (APS), running at 60 keV (λ = 0.414 Å), with samples ground under N_2, sieved to 90 μm, and sealed under N_2 in 0.5-mm-diameter glass capillaries. Rietveld refinements were conducted using the EXPGUI frontend for GSAS.[49,50]

X-ray total scattering was performed at beamline 11-ID-B at the APS, using the sample heater described by Chupas,[51] with samples in 0.7-mm-diameter quartz capillaries sealed under vacuum. Data were collected at 90 keV, and a maximum momentum transfer was chosen at Q_{max} = 20 Å^{-1} for Fourier transformation of the total scattering function $S(Q)$ to the PDF using the PDFgetX2 software.[52] Least-squares refinements were performed using PDFgui.[53]

Reverse Monte Carlo simulations were run using the RMCProfile package[54] running on single 2 GHz cores. Supercells of K_2S_5 were created using 9×9×3 unit cells of the $P2_12_12_1$ average structure, for a total of 6804 atoms in a box of dimensions 58 × 59 × 52 Å. Hard-sphere nearest-neighbor cutoffs were placed at 1.88, 2.70, and 3.30 Å for S−S, K−S, and K−K, respectively, but no bunching was observed at these distances. Atomic visualization presented here is output using VESTA.[55]

Raman spectroscopy was performed using a Renishaw inVia Raman microscope, utilizing a 532-nm laser. High-temperature *in situ* spectra

dx.doi.org/10.1021/ja303047e | J. Am. Chem. Soc. 2012, 134, 9456−9463

were recorded using a Linkam TMS600 heating stage. Samples were sealed under vacuum in 0.5-mm-diameter glass capillaries and placed flat on the heating stage with a heating rate of 20 °C/min. Preliminary experiments were conducted to ensure that the laser power was modest enough (5% power, 20 s exposures) to avoid significant local heating of the sample. No changes in Raman spectra were observed during 20 min spent at 400 °C.

RESULTS AND DISCUSSION

Structural Refinements. Phase purity of K_2S_3 and K_2S_5 synthesized using the crucible-in-tube technique was confirmed using Rietveld refinements to powder X-ray diffraction data, shown in Figure 3. The unit cells of K_2S_3 and K_2S_5 are shown in Figure 2. Each consists of S_3^{2-} or S_5^{2-} chains, separated by lone K^+ ions. The phase diagram of Sangster[32] (Figure 1) and our high-temperature X-ray diffraction confirm that both these phases melt congruently. This implies that, for compounds K_2S_n, where $n \leq 6$, the S_n^{2-} chains persist at least to the point of melting.

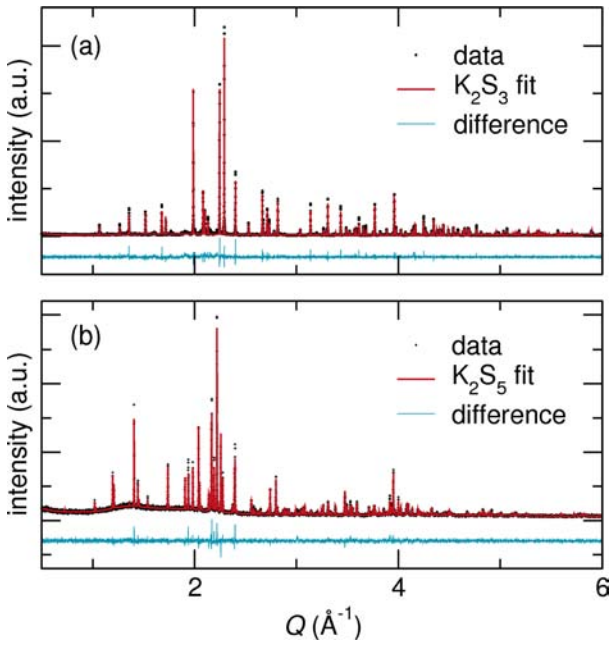

Figure 3. Rietveld refinements to (a) K_2S_3 and (b) K_2S_5 synchrotron powder diffraction data from APS beamline 11-BM, confirming the phase purity of samples synthesized by a crucible-in-tube method.

***In Situ* Raman Spectroscopy.** Raman spectroscopy is an excellent tool for the study of molten salts because *in situ* studies are accessible, and the work of Janz et al. has shown that the measured room-temperature spectra of solid K_2S_n ($1 \leq n \leq 6$) are distinct.[40] Lengthening of the S_n^{2-} chains should lead to salient differences between the chains in the melt.[30] Our room-temperature Raman spectra for K_2S_3 and K_2S_5 are shown in Figure 4. These samples were confirmed to be phase-pure by Rietveld refinement in Figure 3, and they agree with the published spectra. Peaks in the 400−500 cm^{-1} range correspond to S−S stretching modes of the S_n^{2-} chains.[40]

When K−S and Na−S batteries were under heavy investigation, attempts were made to use thermodynamic knowledge of the systems to estimate S_n^{2-} chain lengths in the melt and thereby explain the electromotive force across Na−S cells.[56−58] Cleaver and Sime's investigation of Na_2S_n proposed a broad distribution of S_n^{2-} chain lengths, smoothly varying for $2 < n < 6$ at 300 °C.[36] In this case, where a wide distribution of S_n^{2-} species would be present in the melt, the Raman spectra should be smoothly varying from molten K_2S_3 to K_2S_5, with all modes present and in gradually shifting intensity.

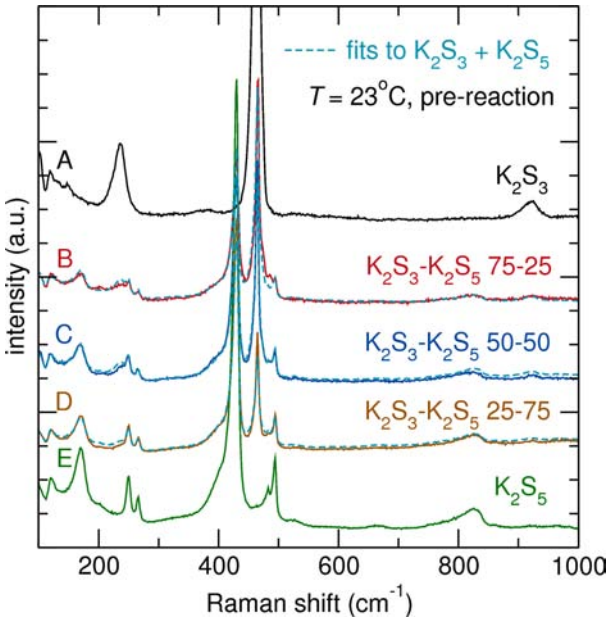

Figure 4. Room-temperature Raman spectra of as-synthesized K_2S_3 (top), K_2S_5 (bottom) and mixtures of the two samples at varying molar ratios, before *in situ* reaction. Dashed fits are weighted averages of K_2S_3 and K_2S_5. Samples are labeled A−E to emphasize continuity across all Raman data presented here.

If, however, liquid polysulfides of exact K_2S_n stoichiometry have a strong preference to form chains of only length n, the Raman spectrum of each melt with integer n should be distinct, just as they are for each of the solid phases.

To test the two models (large n distribution versus precise chains of length n), powders of pure K_2S_3 and K_2S_5 were ground and mixed at K_2S_3/K_2S_5 atomic ratios of 75−25, 50−50 (corresponding to an average compositions of K_2S_4), and 25−75. The Raman spectra of the powder mixtures at room temperature are shown in Figure 4. In all Raman spectra presented here, each sample is designated A−E (in order of increasing S content) to emphasize that they correspond to the *same samples* at different stages of *in situ* reaction. Only modes from K_2S_3 and K_2S_5 are seen at room temperature. Dashed lines in Figure 4 are fits to linear combinations of K_2S_3 and K_2S_5 (c_AA + c_EE), where c_i is the weighting and $\sum c_i = 1$. Upon heating, these mixtures melt and react.

At 400 °C, the range of compositions between K_2S_3 and K_2S_5 are all molten, and fits to the two models were conducted. In the case of a model with a broad distribution of S_n^{2-} lengths, the spectra of the intermediate 25−75, 50−50, and 75−25 compositions should be combinations of modes that are present in the K_2S_3 and K_2S_5 end members (which would be themselves mixtures of many S_n^{2-} chain lengths). An attempt to fit the experimental spectra using this model is shown in Figure 5, where least-squares fits to the data were made using a linear combination of the experimental K_2S_3 and K_2S_5 spectra (c_AA + c_EE). Spectrum C at 50−50 composition in particular is very poorly fit, and the model of a wide distribution of S_n^{2-} chain lengths is not supported by Raman spectroscopy.

Fits to the molten K_2S_n Raman spectra using a model where S_n^{2-} chain lengths are tightly bound by the overall

dx.doi.org/10.1021/ja303047e | J. Am. Chem. Soc. 2012, 134, 9456−9463

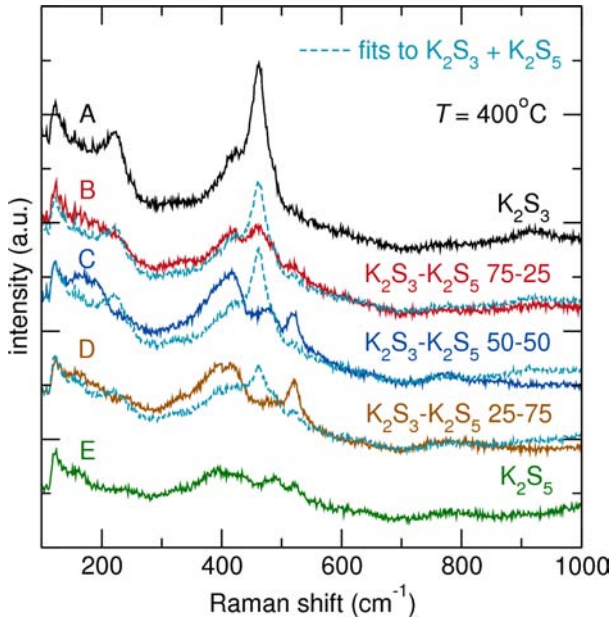

Figure 5. Raman spectra of K_2S_3–K_2S_5 mixtures at T = 400 °C (solid lines), fit using linear combinations (dashed lines) of the K_2S_3 and K_2S_5 spectra. These fits of the type (c_AA + c_EE) do not reproduce the spectra for the mixed compositions, unlike before these samples were subjected to heating (Figure 4), implying that the distribution of S_n^{2-} is not smoothly varying across the series.

stoichiometry (a liquid line compound model) are shown in Figure 6. In this case, the 50–50 composition C must be treated as a distinct K_2S_4 species itself (after all, the glass K_2S_4 appears as a congruently melting phase in the K–S phase diagram in Figure 1). The 25–75 and 75–25 compositions B and D should represent linear combinations of the K_2S_3–K_2S_4 and K_2S_4–K_2S_5 spectra, respectively. These fits can be written

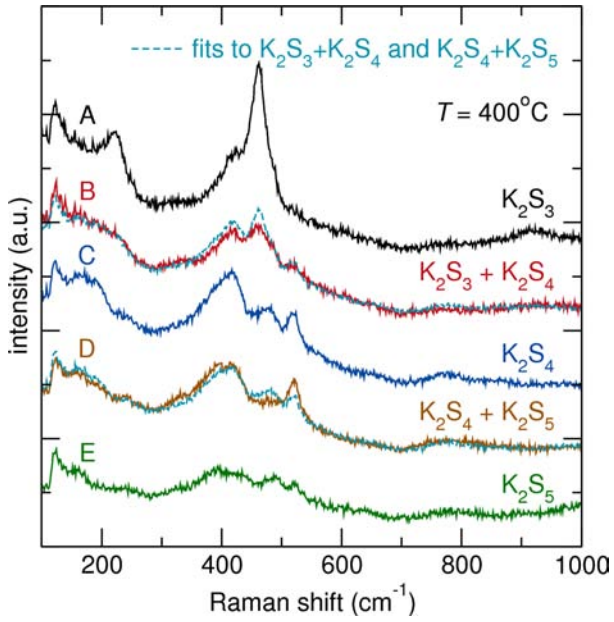

Figure 6. Raman spectra (same data as Figure 5) of K_2S_3–K_2S_5 mixtures at T = 400 °C (solid lines), fit using linear combinations (dashed lines) of the K_2S_3, K_2S_4, and K_2S_5 spectra. The data can be reproduced by assuming that K_2S_4 has a distinct molten structure, as it does in the solid phase.

(c_AA + c_CC) and (c_CC + c_EE) and the agreements in Figure 6 are excellent.

These findings imply that S_n^{2-} chain lengths in molten K_2S_n are coupled to the composition and tuned by temperature. Since this system is a medium for low-temperature crystal growth, the considerations for directed synthesis are profound. The variety of possible species in the melt, and factors influencing their interconversion, may explain why many metastable compounds can be stabilized from polychalcogenide fluxes. The temperature dependence of these relations should vary from T_m, where chain distribution is probably its tightest, to high T, where polyanions must eventually break down. Further Raman spectroscopy should be able to contribute to this area, although signal markedly decreases with temperature.

After cooling to room temperature, the K_2S_3–K_2S_5 mixtures display the Raman spectra in Figure 7, with spectra of the

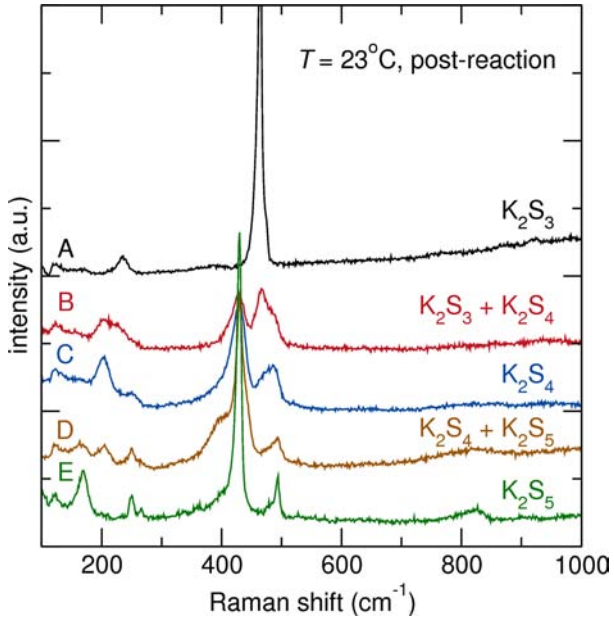

Figure 7. Raman spectra of the polysulfides after cooling, showing formation of K_2S_4, and mixtures with K_2S_3 and K_2S_5.

stoichiometric n = 3, 4, and 5 compounds all matching those reported by Janz.[40] The intermediate compositions B and D correspond to mixtures of K_2S_3–K_2S_4 and K_2S_4–K_2S_5. In the solid state, these are line compounds as prescribed by the phase diagram in Figure 1. In the melt, this composition-structure relationship extends to the tight distributions of S_n^{2-} chains.

Assignment of the exact polysulfide species responsible for modes in the molten Raman spectra is nontrivial because S_n^{2-} in the flux are very different from the isolated, gas-phase molecules amenable to electronic structure calculations.[31] However, local coordination can be probed by the PDF, where a direct measurement of the real-space structure of melts is possible.

***In Situ* X-ray Total Scattering and Local Structure.** X-ray total scattering data were collected up to 400 °C in order to probe the local structure of molten K_2S_5. PDF techniques provide an excellent complement to Raman since the information is purely structural, not spectroscopic, while still describing local interactions.[59–61] The PDF of pure K_2S_5 at room temperature in Figure 8 was fit using a least-squares refinement to the $P2_12_12_1$ average structure. This least-squares

dx.doi.org/10.1021/ja303047e | J. Am. Chem. Soc. 2012, 134, 9456–9463

agreement also precludes the existence of glassy K_2S_4 or K_2S_6 impurities.

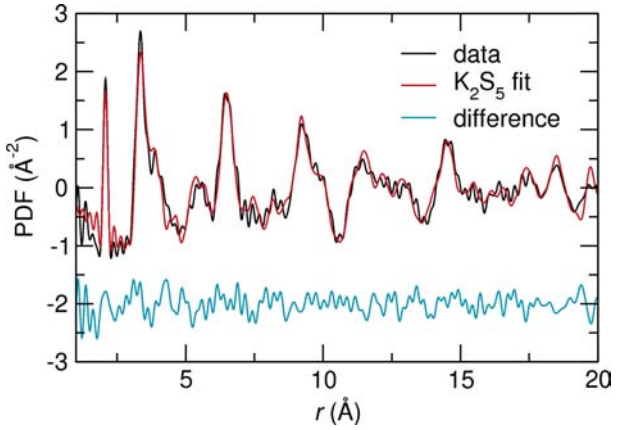

Figure 8. Room-temperature PDF least-squares refinement of K_2S_5, showing a pure phase. The peak at r = 2 Å corresponds to S−S bonding.

As K_2S_5 is heated past melting, loss of long-range structure causes details in the PDF at higher r to disappear. This progression is shown in Figure 9. The S−S nearest-neighbor

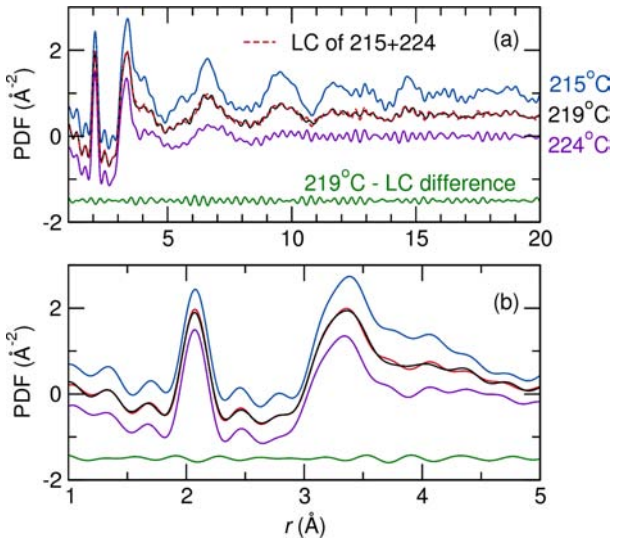

Figure 9. K_2S_5 PDF in the vicinity of melting, showing a loss of long-range structure from 215 to 224 °C. The linear combination (LC, dashed) of the 215 and 224 °C data reproduces the data from 219 °C, showing that K_2S_5 is congruently melting. Difference curve of the 219 °C data minus LC is shown below. Data curves offset by ±1 for clarity.

peak at r = 2.07 Å remains sharp, but farther correlations outside r > 4 Å weaken. The PDFs above and below the melting temperature can be averaged (best fit within 1% of even weighting) to precisely reproduce the intermediate PDF at 219 °C in Figure 9. Only K_2S_5 is present, so we confirm that it is congruently melting. For K_2S_5, T_m = 204 °C; this difference can be attributed to the extra quartz tube encasing the sample and overheating due to the 10 °C/min heating rate.

In the context of our results from Raman spectroscopy, we wish to see whether S_5^{2-} chains in the crystalline solid persist into the melt, and whether the PDF is a viable way of probing distinct S_n^{2-} species. Determining whether our measured PDFs contain enough information to probe S_5^{2-} chains in molten K_2S_5 is a difficult task since (i) the distance between the ends of the chain is 5.16 Å at room temperature, and the PDF contains many correlations of r < 5.16 Å (including interatomic distances to neighboring chains which are not of interest) that effectively comprise a high amount of noise and (ii) the S_n^{2-} chains may exhibit rotations around S−S bonds and stretch at each position, leading to a broad distribution of possible distances between the ends of chains in the melt.

Since the K_2S_5 melt is devoid of long-range symmetry and may contain an infinite variety of chain conformations, small-box modeling such as the least-squares refinement of the K_2S_5 unit cell in Figure 8 cannot faithfully model the S_n^{2-} chain lengths in the melt. Instead, we turned to RMC modeling of the PDF, which is invaluable for the modeling of disordered structures from total scattering data.[46,48]

In order to test the sensitivity of the molten K_2S_5 PDF data to S_n^{2-} chain length, we prepared two disparate models: one where S are required to maintain S_5^{2-} chains at all times (strongly constrained, as our Raman suggests), and one where randomly distributed S are driven by the data to segregate freely into S_n^{2-}.

In the first model, the K_2S_5 unit cell (where all S are in S_5^{2-} chains) was tiled to create a 9×9×3 supercell, and constraints were applied during RMC simulation that require S_5^{2-} to always remain intact and precisely of length n = 5. This was accomplished by creating "distance window" constraints where S chain-end atoms are allowed one and only one neighbor closer than 2.31 Å, and chain-middle S atoms are restricted to precisely two neighbors within 1.88−2.31 Å. The PDF of the starting configuration (containing very sharp peaks since no experimental broadening is applied) is shown in the top of Figure 10a. After fitting this highly restrained model to the data using RMC, the experimental PDF was reproduced very well, as

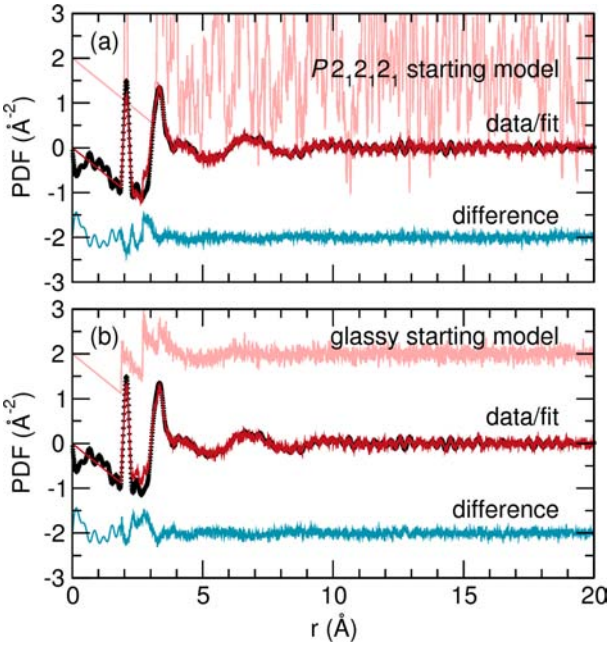

Figure 10. RMC fits to 224 °C PDF data starting from (a) the average $P2_12_12_1$ K_2S_5 structure (the undisturbed crystalline starting model gives an overly sharp PDF) and (b) a random glass, as described in the text. After RMC, both models fit the data equally well, despite S_5^{2-} being constrained in (a) and unconstrained in (b).

dx.doi.org/10.1021/ja303047e | J. Am. Chem. Soc. 2012, 134, 9456−9463

shown in Figure 10a. This agreement implies that our Raman findings can be supported by PDF data. However this rigid S_5^{2-} model is not necessarily a unique solution—the unconstrained model must be considered.

The unconstrained model was created using a supercell of the same dimensions, and populated by placing K and S atoms completely at random, with the only constraint being the hard-shell nearest-neighbor cutoffs common to all simulations (specified in the Experimental Procedure). The result is a glassy, albeit chemically unreasonable, supercell. The PDF of the random model is shown in the top of Figure 10b. There are no features in the starting model that resemble the S−S or K−S correlations of $r < 4$ Å. This model was used as a starting point for RMC simulation and the experimental PDF was reproduced, as shown in the middle of Figure 10b. The S−S peak at $r = 2.07$ Å is fit by RMC, so the increase in S−S correlations should be commensurate with formation of S_n^{2-} chains in this melt. The question is whether these unconstrained fits have converged to the same distribution of S_n^{2-} chain lengths as the highly constrained S_5^{2-} model.

Statistical analysis of the S_n^{2-} chain lengths (taken to be any string of S atoms connected by <2.31 Å) in the glassy model after RMC fitting gives the histogram of S_n^{2-} chains in Figure 11a. The finished model contains a large number of lone S

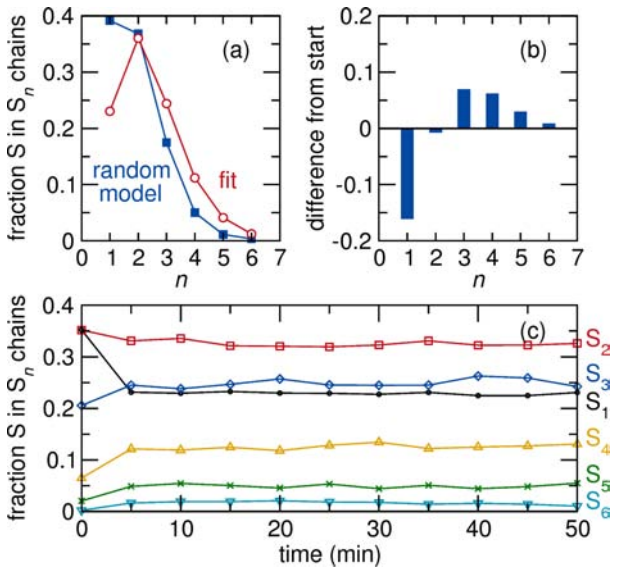

Figure 11. (a) S_n^{2-} chain length histograms for the unconstrained glassy model before and after RMC fitting to data. The differences between the starting and ending histograms are given in (b). Fractions of lone and dimerized sulfur atoms decrease while longer chains grow. Results are averages of five independent simulations. (c) Distribution of chain lengths versus fitting time, showing oscillation around their final values after only 5 min, implying that these simulations will never converge to a model where long S_5^{2-} chains are favored.

atoms and S_2^{2-} dimers, which is not thermodynamically reasonable.[31] For comparison the S_n^{2-} histogram of the starting random model before RMC is shown.

The difference in the histogram of S_n^{2-} chain lengths in the supercell after RMC fitting is shown in Figure 11b. Indeed, the number of lone sulfur atoms and dimer S_2^{2-} decreased while all chains of $n \geq 3$ became more prevalent. The approach to an equilibrium distribution of chain lengths can be seen in the plot of S_n^{2-} chain lengths as a function of RMC fitting time in Figure 11c. After only 5 min of a 10-h simulation, the chain lengths have begun to fluctuate around the final average values. There is no trend toward formation of S_5^{2-} in particular. Instead, most S are contained in S_2^{2-} dimers. This trend of "locking-in" a disordered arrangement has been seen before in RMC studies of amorphous materials,[62] and techniques exist to impose similar local environments on equivalent atoms during the simulation.[63] It remains to be seen whether polyanionic fluxes might obey such constraints.

Because the S_5^{2-}-constrained model and the random glass model fit the data equally well but do not converge on a similar answer, we can say that our experimental PDF requires additional, independent information to definitively specify the length (or distribution of lengths) of S_n^{2-} in the melt. In our study, Raman spectroscopy fills this role. Nevertheless we propose that this method of extracting chain lengths from RMC modeling of total scattering data may prove valuable for identifying other molten chemical species, especially if the cluster of interest is small. Early total scattering studies found signatures of Zintl polyanions in the A-Sn, and A-Te systems[64−66] (where A is an alkali metal), both of which are viable fluxes for crystal growth.[15,67,68] Constraints on the number of distinct anion coordinations might be gleaned from X-ray absorption spectroscopy or nuclear magnetic resonance, although the latter is not straightforward for sulfides.[69]

Implications for Future Experiments. Equipment and methods are available for *in situ* crystal growth experiments in molten fluxes. High-temperature Bragg diffraction indicates flux melting, crystal formation, and conversion between metastable phases. If cations fully dissolve, additional probes of local structure are necessary to monitor changes in the flux and identify the solute complex. For these purposes PDF and Raman analysis are complementary. Best for rigid species and nanoscale precipitates, the PDF gives quantitative coordination information and describes the real-space local structure and extent of crystalline ordering.

Raman spectroscopy is sensitive to solute complexation, and we show here that changes in the flux itself are evident in the vibrational spectra. If structural motifs from the flux (polyanions) are incorporated into the product, it may be possible to monitor their depletion from the melt. The changes in spectra of molten K_2S_3 to K_2S_5 imply that Raman may serve as a monitor of the A/Q ratio, which defines the basicity of the flux and has been seen to define the crystalline product in many systems.[5,28]

When reagents are introduced to any reactive flux, new bonds appear and corresponding modes in the flux spectra should be evident. A special case occurs if the reagents are solvated before the formation of a long-range ordered phase. In that critical regime it may be possible to guide the complexes into new or metastable structures. We hope to examine these scenarios in the near future.

■ CONCLUSIONS

We have investigated potassium polysulfides at conditions relevant to crystal growth in order to gain an understanding of their behavior and to determine viable methods of probing the stability and local structure of their constituent S_n^{2-} species. K_2S_3 and K_2S_5 were prepared by a crucible-in-tube vapor transport method. Raman spectroscopy was performed *in situ* at 400 °C for samples in the compositional range between K_2S_3 and K_2S_5. It was necessary to treat the K_2S_4 composition as possessing molten species that are separate from those in K_2S_3

dx.doi.org/10.1021/ja303047e | J. Am. Chem. Soc. 2012, 134, 9456−9463

and K_2S_5. This implies that S_n^{2-} species present in the melt are strongly coupled for compositions *n*. This dependence of local structure on stoichiometry may influence mechanisms of crystal growth in these media. The temperature range over which this relationship holds should be investigated. At 400 °C we do not find a broad distribution of molten polysulfide chain lengths where S_n^{2-} are in equilibrium with S_{n-1}^{2-}, S_{n+1}^{2-}, etc., as was originally proposed to explain the electromotive force of Na_2S_n batteries.[36]

Analysis of the PDF obtained from X-ray total scattering indicated that the chain distributions in K_2S_5 are not readily visible. Reverse Monte Carlo fits to these data revealed that the PDF of K_2S_5 requires additional information to distinguish the species present. However, the chain-building techniques presented here may be useful for determining the more rigid species in melts or amorphous materials.

We have discussed the viability of PDF analysis and Raman spectroscopy for future studies probing crystal growth in molten fluxes, with the ultimate goal of understanding and controlling synthetic reaction mechanisms.

AUTHOR INFORMATION

Corresponding Author

m-kanatzidis@northwestern.edu

Notes

The authors declare no competing financial interest.

ACKNOWLEDGMENTS

The authors thank Troy Lutes and the APS Detector Pool for providing the heating stage for the Raman microscope. We also thank Suntharalingam Skanthakumar and Richard E. Wilson with assistance during data collection, and Kevin Beyer and Melanie Francisco for experimental assistance and helpful discussion. Argonne National Laboratory, a U.S. Department of Energy Office of Science Laboratory, is operated by UChicago Argonne, LLC, under contract No. DE-AC02-06CH211357.

REFERENCES

(1) (a) Kanatzidis, M. G. *Chem. Mater.* **1990**, *2*, 353−363. (b) Park, Y. B.; Kanatzidis, M. G. *Angew. Chem., Int. Ed. Engl.* **1990**, *29*, 914−915.

(2) Kanatzidis, M. G.; Sutorik, A. C. *Prog. Inorg. Chem.* **1995**, *43*, 151−265.

(3) Kanatzidis, M. G. *Curr. Opin. Solid State Mater. Sci.* **1997**, *2*, 139−149.

(4) Stoll, P.; Näther, C.; Bensch, W. *Z. Anorg. Allg. Chem.* **2002**, *628*, 2489−2494.

(5) Palchik, O.; Marking, G. M.; Kanatzidis, M. G. *Inorg. Chem.* **2005**, *44*, 4151−4153.

(6) Deng, B.; Chan, G. H.; Huang, F. Q.; Gray, D. L.; Ellis, D. E.; Van Duyne, R. P.; Ibers, J. A. *J. Solid State Chem.* **2007**, *180*, 759−764.

(7) Wu, Y.; Bensch, W. *Inorg. Chem.* **2009**, *48*, 2729−2731.

(8) Graf, C.; Assoud, A.; Mayasree, O.; Kleinke, H. *Molecules* **2009**, *14*, 3115−3131.

(9) Wu, Y.; Bensch, W. *Z. Naturforsch. A* **2010**, *65b*, 1219−1228.

(10) Chung, I.; Biswas, K.; Song, J.; Androulakis, J.; Chondroudis, K.; Paraskevopoulos, K. M.; Freeman, A. J.; Kanatzidis, M. G. *Angew. Chem., Int. Ed.* **2011**, *50*, 8834−8838.

(11) Wu, Y.; Bensch, W. *J. Alloys Compd.* **2011**, *509*, 4452−4456.

(12) Liao, J. H.; Kanatzidis, M. G. *Chem. Mater.* **1993**, *5*, 1561−1569.

(13) Bera, T. K.; Song, J.; Freeman, A.; Jang, J.; Ketterson, J.; Kanatzidis, M. *Angew. Chem.* **2008**, *120*, 7946−7950.

(14) Bera, T. K.; Jang, J. I.; Song, J.; Malliakas, C. D.; Freeman, A. J.; Ketterson, J. B.; Kanatzidis, M. G. *J. Am. Chem. Soc.* **2010**, *132*, 3484−3495.

(15) Chung, D.; Hogan, T.; Brazis, P.; Rocci-Lane, M.; Kannewurf, C.; Bastea, M.; Uher, C.; Kanatzidis, M. G. *Science* **2000**, *287*, 1024−1027.

(16) Kyratsi, T.; Chung, D.; Ireland, J. R.; Kannewurf, C. R.; Kanatzidis, M. G. *Chem. Mater.* **2003**, *15*, 3035−3040.

(17) Sankar, C. R.; Bangarigadu-Sanasy, S.; Assoud, A.; Kleinke, H. *J. Mater. Chem.* **2010**, *20*, 7485−7490.

(18) Sankar, C. R.; Bangarigadu-Sanasy, S.; Kleinke, H. *J. Electron. Mater.* **2012**, DOI: 10.1007/s11664-011-1846-z.

(19) Lekse, J. W.; Moreau, M. A.; McNerny, K. L.; Yeon, J.; Halasyamani, P. S.; Aitken, J. A. *Inorg. Chem.* **2009**, *48*, 7516−7518.

(20) Mei, D.; Lin, Z.; Bai, L.; Yao, J.; Fu, P.; Wu, Y. *J. Solid State Chem.* **2010**, *183*, 1640−1644.

(21) Mei, D.; Yin, W.; Feng, K.; Lin, Z.; Bai, L.; Yao, J.; Wu, Y. *Inorg. Chem.* **2011**, *51*, 1035−1040.

(22) Manos, M. J.; Chrissafis, K.; Kanatzidis, M. G. *J. Am. Chem. Soc.* **2006**, *128*, 8875−8883.

(23) Manos, M.; Kanatzidis, M. *Chem.—Eur. J.* **2009**, *15*, 4779−4784.

(24) Axtell, E. A., III; Liao, J.; Pikramenou, Z.; Kanatzidis, M. G. *Chem.—Eur. J.* **1996**, *2*, 656−666.

(25) Androulakis, J.; Peter, S. C.; Li, H.; Malliakas, C. D.; Peters, J. A.; Liu, Z.; Wessels, B. W.; Song, J.; Jin, H.; Freeman, A. J.; Kanatzidis, M. G. *Adv. Mater.* **2011**, *23*, 4163−4167.

(26) Axtell, E. A., III; Park, Y.; Chondroudis, K.; Kanatzidis, M. G. *J. Am. Chem. Soc.* **1998**, *120*, 124−136.

(27) Nguyen, S. L.; Jang, J. I.; Ketterson, J. B.; Kanatzidis, M. G. *Inorg. Chem.* **2010**, *49*, 9098−9100.

(28) Dürichen, P.; Bensch, W. *Z. Naturforsch. B, Chem. Sci* **2002**, *57*, 1382−1386.

(29) Berghof, V.; Sommerfeld, T.; Cederbaum, L. S. *J. Phys. Chem. A* **1998**, *102*, 5100−5105.

(30) Rouquette, C.; Digne, M.; Renaudot, L.; Grandjean, J.; Ballaguet, J. *Energy Fuels* **2009**, *23*, 4404−4412.

(31) Steudel, R. *Top. Curr. Chem.* **2003**, *231*, 127−152.

(32) Sangster, J.; Pelton, A. D. *J. Phase Equilib.* **1997**, *18*, 82−88.

(33) Chung, D.; Iordanidis, L.; Choi, K. S.; Kanatzidis, M. G. *Bull. Kor. Chem. Soc.* **1998**, *19*, 1283−1293.

(34) Evenson; Dorhout, P. K. *Inorg. Chem.* **2001**, *40*, 2409−2414.

(35) Selby, H. D.; Chan, B. C.; Hess, R. F.; Abney, K. D.; Dorhout, P. K. *Inorg. Chem.* **2005**, *44*, 6463−6469.

(36) Cleaver, B.; Sime, S. *Electrochim. Acta* **1983**, *28*, 703−708.

(37) McKubre, M. C. H.; Tanzella, F. L.; Smedley, S. I. *J. Electrochem. Soc.* **1989**, *136*, 303−305.

(38) Cleaver, B.; Davies, A.; Hames, M. *Electrochim. Acta* **1973**, *18*, 719−726.

(39) Cleaver, B.; Davies, A. *Electrochim. Acta* **1973**, *18*, 727−731.

(40) Janz, G. J.; Coutts, J. W.; Downey, J. R.; Roduner, E. *Inorg. Chem.* **1976**, *15*, 1755−1759.

(41) Janz, G. J.; Downey, J. R.; Roduner, E.; Wasilczyk, G. J.; Coutts, J. W.; Eluard, A. *Inorg. Chem.* **1976**, *15*, 1759−1763.

(42) El Jaroudi, O.; Picquenard, E.; Demortier, A.; Lelieur, J.; Corset, J. *Inorg. Chem.* **1999**, *38*, 2394−2401.

(43) El Jaroudi, O.; Picquenard, E.; Demortier, A.; Lelieur, J.; Corset, J. *Inorg. Chem.* **2000**, *39*, 2593−2603.

(44) Pinon, V.; Lelieur, J. P. *Inorg. Chem.* **1991**, *30*, 2260−2264.

(45) Billinge, S. J. L.; Kanatzidis, M. G. *Chem. Commun.* **2004**, 749−760.

(46) Keen, D. A.; McGreevy, R. L. *Nature* **1990**, *344*, 423−425.

(47) McGreevy, R. L. *Nuovo Cim. D* **1990**, *12*, 685−701.

(48) McGreevy, R. L. *Int. J. Mod. Phys. B* **1993**, *7*, 2965−2980.

(49) Larson, A.; Von Dreele, R. *Los Alamos National Lab. Rep.* **2000**, *86*, 748.

(50) Toby, B. H. *J. Appl. Crystallogr.* **2001**, *34*, 210−213.

(51) Chupas, P. J.; Chapman, K. W.; Kurtz, C.; Hanson, J. C.; Lee, P. L.; Grey, C. P. *J. Appl. Crystallogr.* **2008**, *41*, 822−824.

(52) Qiu, X.; Thompson, J. W.; Billinge, S. J. L. *J. Appl. Crystallogr.* **2004**, *37*, 678−678.

(53) Farrow, C. L.; Juhas, P.; Liu, J. W.; Bryndin, D.; Bozin, E. S.; Bloch, J.; Proffen, T.; Billinge, S. J. L. *J. Phys. Cond. Mat.* **2007**, *19*, 335219.
(54) Tucker, M. G.; Keen, D. A.; Dove, M. T.; Goodwin, A. L.; Hui, Q. *J. Phys. Cond. Mat.* **2007**, *19*, 335218.
(55) Momma, K.; Izumi, F. *J. Appl. Crystallogr.* **2008**, *41*, 653−658.
(56) Crosbie, G. M. *J. Electrochem. Soc.* **1982**, *129*, 2707−2711.
(57) Lindberg, D.; Backman, R.; Hupa, M.; Chartrand, P. *J. Chem. Thermodyn.* **2006**, *38*, 900−915.
(58) Morachevskii, A. G.; Maiorova, E. A. *Russ. J. Appl. Chem.* **2002**, *75*, 1580−1584.
(59) Goodwin, A. L.; Tucker, M. G.; Cope, E. R.; Dove, M. T.; Keen, D. A. *Phys. Rev. B* **2005**, *72*, 214304.
(60) Shoemaker, D. P.; Li, J.; Seshadri, R. *J. Am. Chem. Soc.* **2009**, *131*, 11450−11457.
(61) Shoemaker, D. P.; Seshadri, R.; Hector, A. L.; Llobet, A.; Proffen, T.; Fennie, C. J. *Phys. Rev. B* **2010**, *81*, 144113.
(62) Gereben, O.; Pusztai, L. *Phys. Rev. B* **1994**, *50*, 14136−14143.
(63) Cliffe, M. J.; Dove, M. T.; Drabold, D. A.; Goodwin, A. L. *Phys. Rev. Lett.* **2010**, *104*, 125501.
(64) Fortner, J.; Saboungi, M.; Enderby, J. E. *Phys. Rev. Lett.* **1992**, *69*, 1415−1418.
(65) Reijers, H. T. J.; Saboungi, M.; Price, D. L.; van der Lugt, W. *Phys. Rev. B* **1990**, *41*, 5661−5666.
(66) Saboungi, M.; Fortner, J.; Richardson, J.; Petric, A.; Doyle, M.; Enderby, J. *J. Non-Cryst. Solids* **1993**, *156−158*, 356−361.
(67) Hahn, S. E.; Lee, Y.; Ni, N.; Canfield, P. C.; Goldman, A. I.; McQueeney, R. J.; Harmon, B. N.; Alatas, A.; Leu, B. M.; Alp, E. E.; Chung, D. Y.; Todorov, I. S.; Kanatzidis, M. G. *Phys. Rev. B* **2009**, *79*, 220511.
(68) Johnsen, S.; Peter, S. C.; Nguyen, S. L.; Song, J.; Jin, H.; Freeman, A. J.; Kanatzidis, M. G. *Chem. Mater.* **2011**, *23*, 4375−4383.
(69) Jakobsen, H. J.; Bildsøe, H.; Skibsted, J.; Brorson, M.; Srinivasan, B. R.; Näther, C.; Bensch, W. *Phys. Chem. Chem. Phys.* **2009**, *11*, 6981−6986.